Self-cleaving ribozymes conserved in RNA viruses unveil a new role in protein translation

María José López-Galiano[1], Sotaro Chiba[2], Marco Forgia[3], Beatriz Navarro[4], Amelia Cervera[1], Artem Babaian[5,6], Francesco Di Serio[4], Massimo Turina[7], Marcos de la Peña[1*]

[1] Instituto de Biología Molecular y Celular de Plantas, Universidad Politécnica de Valencia-CSIC, Valencia, Spain

[2] Graduate School of Bioagricultural Sciences, Nagoya University, Chikusa, Nagoya, Japan

[3] Institute for Sustainable Plant Protection, National Research Council of Italy, Torino, Italy

[4] Institute for Sustainable Plant Protection, National Research Council of Italy, Bari, Italy

[5] Department of Molecular Genetics, University of Toronto, Toronto, ON, Canada

[6] Terrence Donnelly Centre for Cellular & Biomolecular Research, University of Toronto, Toronto, ON, Canada

[7] Institute for Sustainable Plant Protection, National Research Council of Italy, Brescia, Italy

*corresponding author: rivero@ibmcp.upv.es

Abstract

Small self-cleaving ribozymes are catalytic RNAs originally discovered in viroid-like agents, which are infectious circular RNAs (circRNAs) postulated as relics of a prebiotic RNA world. In the last decade, however, small ribozymes have also been detected across the tree of life, from bacterial to human genomes, and more recently, in viral agents with circRNA genomes. Here we report the conserved occurrence of small ribozymes within the linear genomes of typical ds and ssRNA viruses from fungi and plants. In most 5'-UTR regions of chrysovirids and fusarivirids, we find conserved type I hammerhead ribozymes (hhrbzs) showing efficient self-cleaving activity *in vitro* and *in vivo*. Similar hhrbzs, as well as hepatitis delta and twister ribozymes, were also detected in megabirna-, hypo-, fusagra- and toti-like viruses. These ribozymes occur as isolated motifs but also as close tandem pairs, suggesting that they are involved in the formation of ~300 nt circRNAs. *In vivo* characterization of a chrysovirid hhrbz revealed its unexpected role in protein translation as an internal ribosome entry site (IRES). RNA structural comparison between the hammerhead three-way junction and the core domain of picornavirus IRES elements allow us to suggest that these simple ribozymes may follow a similar strategy to achieve cap-independent translation. We conclude that self-cleaving ribozymes, historically involved in the rolling circle replication of viroid-like agents, have been exapted towards translational functions in linear RNA viruses.

Introduction

RNA's dual nature as carrier of genetic information and biochemical catalyst has established it as a candidate molecule for the origin of life. RNA predates DNA, proteins and the genetic code in the primordial "RNA world" hypothesis[1–3]. Genetic remnants of this hypothetical RNA world would be the extant catalytic RNAs, such as the ribosomal RNAs, the RNAse P, or the small self-cleaving ribozymes. Therefore, the simplest RNA-based entities, such as viruses, viroids and other RNA mobile genetic elements, can be regarded as the living fossils of Earth's first life[4,5]. The simplest known ribozymes belong to the family of small (50-200 nt) self-cleaving RNAs, with nine well characterized members: the hammerhead (hhrbz)[6,7], hairpin (hprbz)[8], human Hepatitis Delta (dvrbz)[9], Varkud-Satellite (vsrbz)[10], glmS[11], twister (twrbz)[12], and twister sister, hatchet and pistol[13] ribozymes. During the '80s, the first small ribozymes were described in infectious circRNAs of plants (hhrbz and hprbz in viroid-like agents), animals (dvrbz in Hepatitis Delta Virus) and fungi (vsrbz in a *Neurospora crassa* plasmid), but also in some DNA genomes[14,15]. In the last decade, these motifs have been discovered to be widespread in the DNA genomes of phages, bacteria, or eukaryotes[16–18], including the human genome[19,20]. The precise biological functions of many of these genomic ribozymes is not well understood, but numerous hhrbz, dvrbz and twrbz motifs strongly associate with autonomous and non-autonomous DNA retrotransposons across plant and metazoan genomes[21–26].

Likely due to its simplicity[27], the hhrbz is one of the most frequent ribozymes detected in nucleic acids. It is composed of three double helixes (I to III) that surround a core of 15 conserved nucleotides, and folds into a γ-shaped helical junction where the loops of helix I and II interact[28,29]. Depending on the open-ended helix, three circularly permuted topologies are possible for the hhrbz (type I, II, or III) (Fig. 1A). The dvrbz, another small ribozyme widespread among DNA genomes, shows a characteristic nested double pseudoknot structure with five helical regions (Fig. 1B).

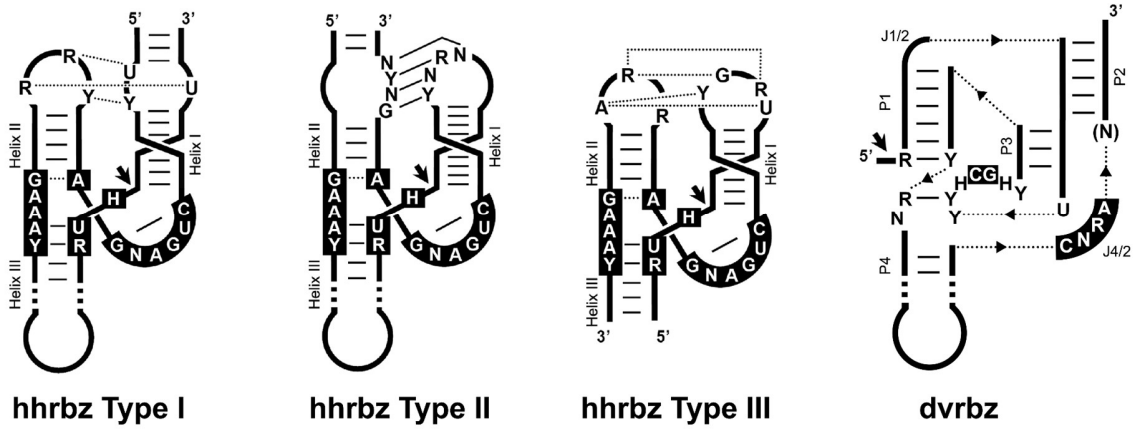

Fig. 1. Schematic representation of the three hammerhead topologies (hhrbz Type I, II, and III) and the hepatitis delta virus (dvrbz) ribozymes. The conserved nucleotides are shown in black boxes. Typical tertiary loop-loop interactions of the hhrbz are indicated (dotted and continuous lines refer to non-canonical and Watson–Crick base pairs, respectively). Dotted lines with triangles represent connections between the helixes. Helical stems and single-stranded junction strands are indicated. Black arrows indicate the self-cleavage site.

Sequencing and computing have driven an exponential growth in the characterized biodiversity of microbial life forms. This expansion has relied on the use of protein hallmark genes or ribosomal RNA. However, we are starting to appreciate the existence of an extant and highly diverse RNA world of minimal agents. Previous analyses have unveiled hundreds of novel circRNA genomes with self-cleaving ribozymes in either one or both polarities[30,31]. More recently, these minimal circRNA agents were expanded to more than 20,000 viroid-like taxonomic units, including examples of novel RNA virus-viroid hybrids such as ambiviruses and some mitoviruses with circular genomes and paired ribozymes[32,33]. This discovery blurs the distinction between viroidal agents, ribozyme-bearing satellite viruses, and RNA viruses, but confirms the existence of a diverse "modern RNA world" of mobile genetic elements with small self-cleaving ribozymes[33].

Here, we extend the conserved occurrence of small self-cleaving ribozymes, notably specific variants of the type I hhrbz, to diverse families of fungal and plant RNA viruses with linear genomes. To our surprise, these motifs do not appear to be involved in the RNA processing of intermediates during rolling-circle replication, but instead have been exapted to perform novel roles in the life cycle of linear RNA viruses.

Results

Type I hammerhead ribozymes in dsRNA viruses

In silico screening for the nine known families of small ribozyme structures in viral sequences deposited in public databases revealed the conserved occurrence of significant motifs across evolutionarily diverse RNA viruses (see Methods for full details). Notably, we identified putative ribozyme motifs in the *Chrysoviridae* family of multipartite dsRNA viruses, where 42% (96 out of 226 contigs >2 kb) of the alphachrysovirus sequences contain a distinct variant of the type I hhrbz class (Fig. 1). These motifs are found in the 5'-UTRs (positive strand) of each of the four RNA segments making up the viral genome (Fig. 2A and Supplementary Table 1). Exceptionally, a few alphachrysoviral segments exhibit a second hhrbz at the 3'-UTR region of the RNA (ie. Raphanus sativus chrysovirus 1, RNA segments 1 and 3. Supplementary Table 1). No examples of hhrbzs or any other ribozymes were detected in any of the betachrysovirus sequences analyzed (134 contigs >2 kb).

Previously described classic type I hhrbzs from eukaryotic retroelements[14,15,22,25,34] usually have a very short/absent helix III, which prevents efficient self-cleavage of monomeric but not of dimeric hhrbz molecules[6,35]. However, in the chrysoviral type I hhrbzs, the helix III is predicted to be longer and more similar to type I hhrbzs encoded in the DNA genomes of bacteria/phages[16], fungi[22] or mammals[19]. The newly uncovered hhrbzs from chrysoviruses can be categorized into two conserved architectures with distinct properties (Fig. 2B); one third of the hhrbzs have a long helix II of 6 bp capped by a tetraloop and usually harboring a bulged adenosine at the middle of the stem, whereas two thirds of the chrysoviral hhrbzs show a very short (1-2 bp stem) or even non-existent helix II (Fig. 2B and Supplementary Fig. 1).

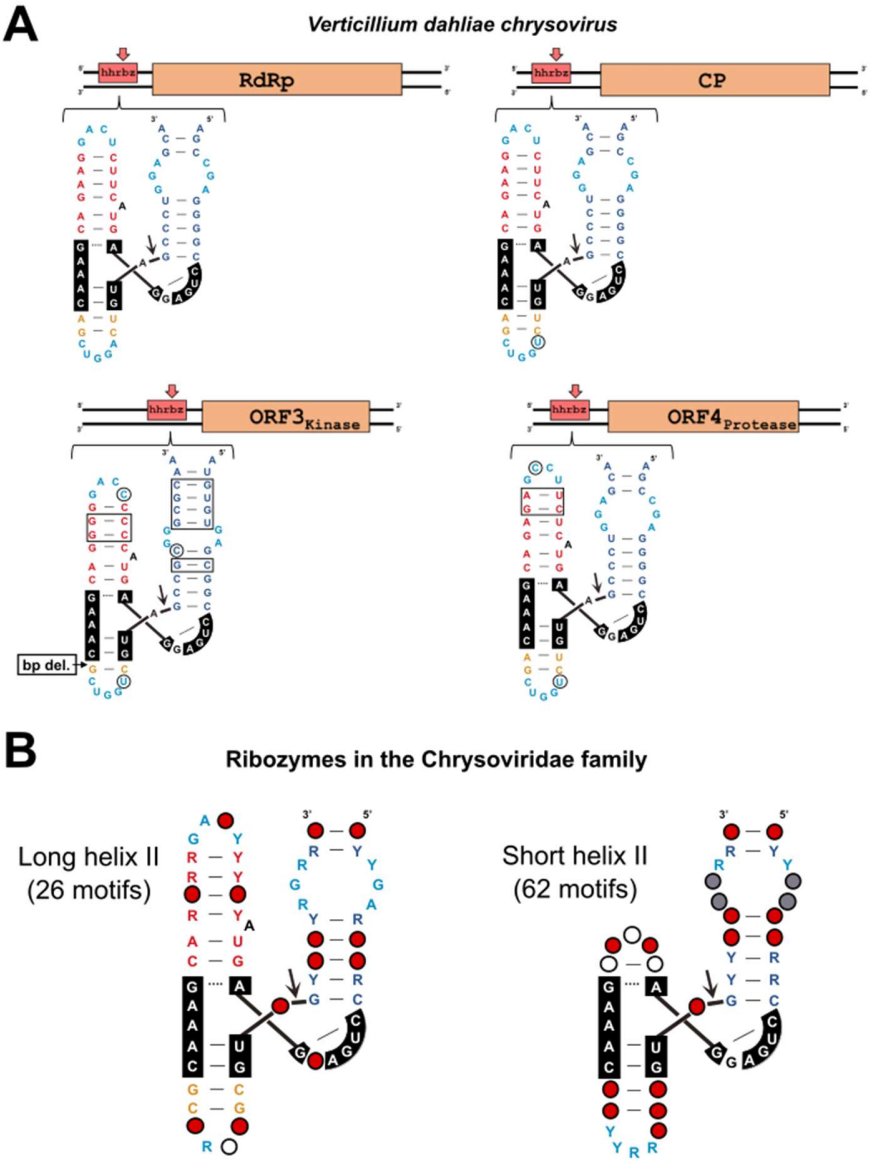

Fig. 2. Fungal and plant chrysovirus hammerhead ribozymes (hhrbz). (A) The multipartite Verticillium dahliae chrysovirus[36]contains type I hhrbzs in the 5'-UTRs of the 4 RNA segments that make up the viral genome. Nucleotide changes in the ribozyme motifs with respect to the hhrbz at the RNA 1 encoding the RNA-dependent RNA polymerase (RdRp) are indicated by circles (single changes) and rectangles (base-pair covariations) (B) A summary of the covariance models for the two hhrbz architectures detected among most chrysoviruses. Red, grey and white dots refer to nucleotides present in more than 97%, 75% or 50% of the sequences, respectively. Y: C or U. R: G or A (See Supplementary Fig. 1A for details). CP, coat protein. ORF, open reading frame.

In vitro analyses confirmed that chrysovirus hhrbzs with long helix II self-cleave efficiently during transcription (k_{obs}~2-3 min^{-1}) (Fig. 3). However, the observed rates of self-cleavage for the hhrbz with short (1 bp) or even absent helix II were low (k_{obs} ~10^{-2} min^{-1}), or very low (k_{obs} ~10^{-3} min^{-1}) respectively, either under co-tanscriptional

or post-transcriptional conditions, even at high pH (8.5) and Mg^{+2} concentrations (10 mM) (Fig. 3, Supplementary Fig. 2).

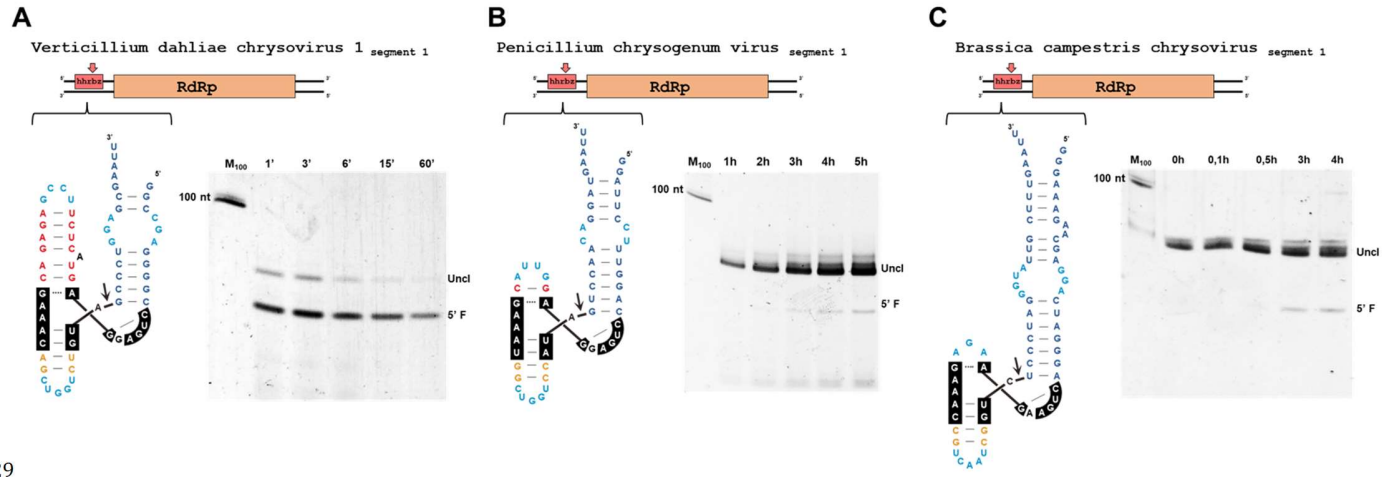

Fig. 3. Self-cleavage kinetics of hammerhead ribozymes from fungal and plant chrysoviruses. (A) long helix II, (B) short helix II, or (C) totally absent helix II hammerhead ribozymes are catalytically competent *in vitro* but show distinct self-cleaving efficiencies. RdRp, RNA-dependent RNA polymerase. (A) and (B) correspond to co-transcriptional cleavage analysis under standard conditions (pH 7.5, 1 mM Mg^{2+}), whereas (C) shows a post-transcriptional assay performed at higher pH (8.5) and Mg^{2+} concentration (10 mM) to increase its self-cleaving capabilities.

Other ds and ssRNA viruses encode hammerhead, but also deltavirus and twister ribozyme motifs

Fusariviruses are a family of mycoviruses with monopartite ssRNA genomes that encode one to four ORFs[37,38]. Our bioinformatic analyses found that up to 114 out of 156 analyzed fusariviral sequences encode one or several type I hhrbzs each (160 hhrbz hits in total) (Supplementary Table 1). The sequences and helix sizes of the motifs are quite variable depending on the viral genome, but as described for chrysoviruses, they either follow a canonical type I hhrbz architecture, with medium size helixes I, II and III (4-8 bp stems), or a variant with a very short helix II (1-2 bp stem) (Supplementary Fig. 1). These observations suggest a high and low self-cleavage efficiency, respectively, for each of the two fusarivirus hhrbz architectures. Again, fusariviral ribozymes occur in the untranslated regions preceding most of the viral ORFs (Fig. 4A and Supplementary Fig. 3A). We made similar observations in the family

of bipartite dsRNA megabirnaviruses[39], which show the presence of slightly different variants of the type I hhrbz with longer helix II (Supplementary Fig. 3B). The motifs occur again in the large 5'-UTR of diverse megabirnavirus RNA segments (17 out of 32 analyzed contigs) (Supplementary Table 1). Interestingly, not only hhrbz motifs, but also an example of a *bonafide* dvrbz was detected in a genomic segment of the Rhizoctonia cerealis megabirnavirus-like RNA (Fig. 4B, Supplementary Fig. 2B). Similarly, instances of dvrbz, as well as type I hhrbz and even examples of twrbz motifs, were detected in the dsRNA genomes of diverse totiviruses. In these examples, however, the motifs were found as pairs of ribozymes (either from the same or different classes) placed in tandem very close to each other (~200-400 nt) (Fig. 4C). This arrangement resembles the one observed in plant and animal retrozymes, where close tandem ribozyme pairs result in the formation of small circular RNAs[24,25]. In the case of totiviruses, the predicted RNA circles can adopt highly stable secondary structures, have nucleotide sizes multiple of 3, and may encode a never-ending polypeptide in their positive polarity (Fig. 4C, Supplementary Fig. 4). The features of these sub-genomic circRNAs are strikingly similar to those described for the intriguing group of viroid-like Zeta viruses detected in diverse environmental metatranscriptomic studies[30,33] (Supplementary Fig. 4). However, most of the predicted circRNAs in totiviruses are not keeping in their sequence any of the two flanking ribozymes (usually a type I hhrbz and a dvrbz at the 5' and 3' ends, respectively), suggesting that they would not be capable of replication through a classic rolling circle mechanism.

Finally, our bioinformatic analyses also revealed the presence of analogous type I hhrbzs in the UTRs of some dsRNA genomes from additional fungal viral families, including fusagraviruses and hypoviruses (Supplementary Table 1). Altogether, these results confirm the prevalence of small self-cleaving ribozymes encoded within the linear ss and dsRNA genomes of diverse fungal and plant viruses.

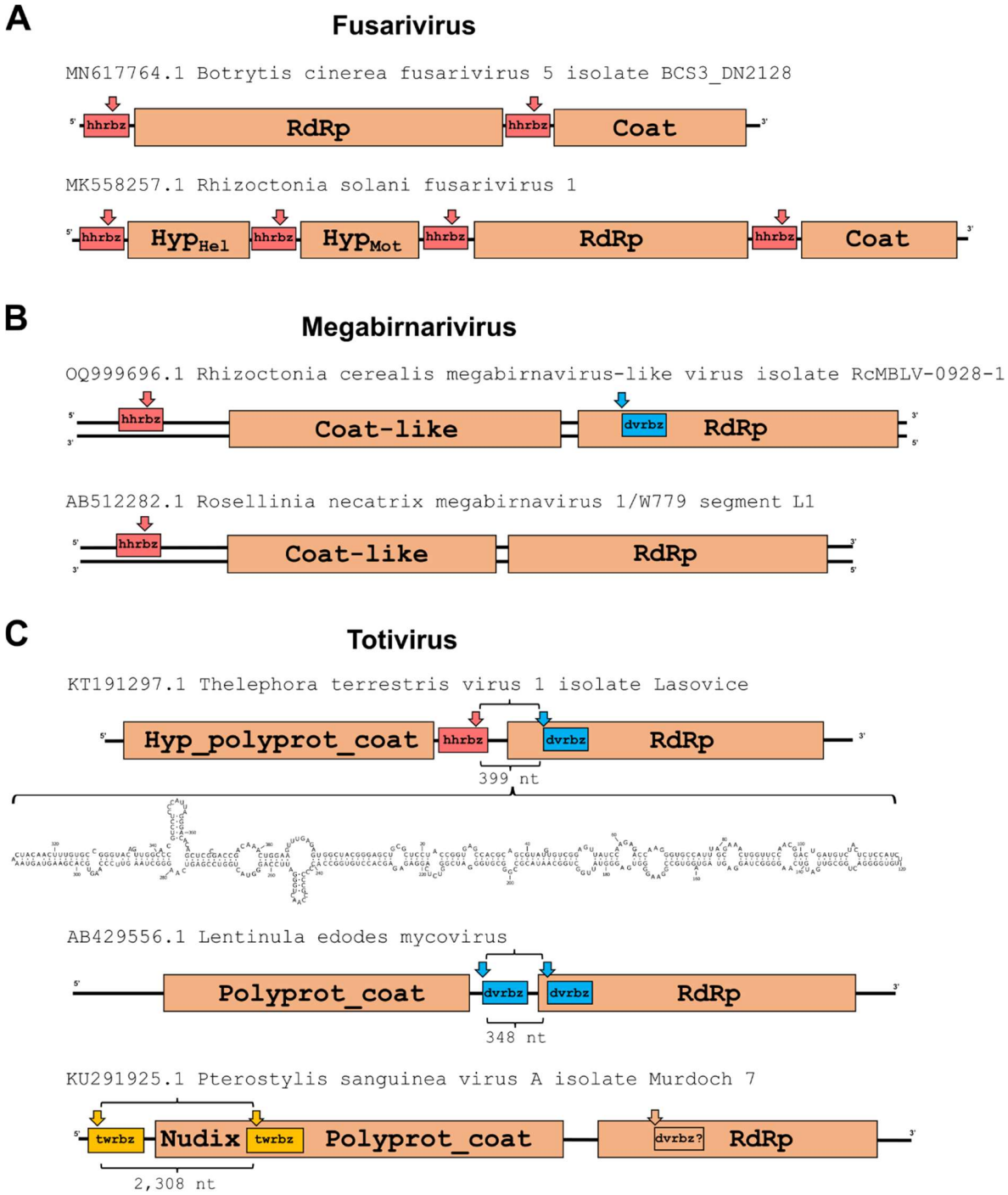

Fig. 4. Small ribozymes are widespread in fungal ss and dsRNA viruses with linear genomes. (A) fusariviruses, (B) megabirnaviruses and (C) totiviruses encode conserved self-cleaving ribozymes of the hhrbz, dvrbz and twrbz classes. In the case of diverse totivirus genomes, pairs of hammerhead and delta self-cleaving ribozymes occur very close to each other (~300 nt). Similar arrangements of close ribozymes in tandem involved in circRNA formation have been previously found encoded in plant (~600 nt[24]) and metazoan (~300 nt[25]) genomes, which suggests that ribozyme pairs in totivirus could allow the formation of similar circular RNAs, as depicted for Telephora terrestris virus 1 (See Supplementary Fig. 4 for more details).

Hammerhead ribozymes in RNA viruses show self-cleaving activity *in vivo*

Given the widespread occurrence of type I hhrbzs among chrysovirids and fusarivirids, we chose to look for *in vivo* evidence of ribozyme self-cleaving activity during viral infection. We selected two chrysoviruses (either infecting a plant or a fungus) and one fungal fusarivirus as examples of ds and ssRNA viruses with hhrbzs in their 5'-UTRs, respectively.

Brassica campestris chrysovirus 1 (BcCV1) is a tripartite dsRNA chrysovirus infecting brassica plants[40], which shows conserved hhrbzs (short helix II variants with a minimal self-cleaving activity *in vitro*, see above) in the 5'-UTRs of each RNA segment. The expected cleavage sites of the hhrbzs map at positions 58, 60 and 60 of RNA segments 1, 2 and 3, respectively (Supplementary Fig. 5A). Rapid amplification of RNA ends (RACE) experiments using total RNA from a BcCV1-infected *B. oleracea* plant generated two amplification products for each of the chrysovirus RNAs, which are more evident in the case of RNA2 and RNA3 (Supplementary Fig. 5B). Cloning and sequencing of the amplicons confirmed the existence, for each genomic RNA segment, of molecules with two different 5' ends, one corresponding to the expected viral full-length RNA segment, and the other one with the self-cleavage site predicted for the respective embedded ribozyme (Supplementary Fig. 5C).

The recently characterized Gnomognopsis castanea chrysovirus 1 (GcCV1) has 4 genomic segments encoding an ORF each, with the exception of the bicistronic RNA3[41]. We detected the presence of 5 different hhrbz motifs (long helix II variants with efficient self-cleaving activity *in vitro*, see above), one in each 5'-UTR preceding an ORF (Supplementary Fig. 6). Here, RACE experiments carried out on total RNA extracted from an infected fungus isolate showed that the population of viral RNAs is also composed of RNA segments with two different 5' termini, as supported by clones either mapping to the expected 5' end of the genomic RNA, or to the predicted 5' site of self-cleavage of each hhrbz (Supplementary Fig. 6). Such a mix of RNA molecules with two different ends is particularly evident for RNA2, which gives two abundant and distinct

bands in PCR RACE amplifications (Supplementary Fig. 6E). It is of note that, in this virus, the two copies of hhrbz present in each one of the two UTRs of the bicistronic RNA3 were found to self-cleave *in vivo* at their predicted sites.

Finally, Pleospora tiphycola fusarivirus 1 (PtFV1) is a ssRNA virus present in an ascomycetes fungus isolated from the seagrass *Posidonia oceanica*[42]. Members of the recently established *Fusariviridae* family are a group of non-segmented viruses with heterogeneous genome organization according to the genus they belong to[38]. The RNA genome of PtFV1 can potentially express up to three proteins from three distinct ORFs[42]. It also contains a predicted hhrbz with a short helix II, quite similar to the Penicilium chrysogenum virus ribozyme (Fig. 3B). The catalytic RNA essentially spans the entire small intergenic UTR (66 nt), with the self-cleavage site (position 4,735) just 7 nucleotides upstream of the proposed ORF2 start codon (position 4,742). RACE analysis using reverse transcription products primed around 200 nt downstream the cutting site confirmed the existence *in vivo* of an RNA species with the predicted 5' end after self-cleavage (Supplementary Fig. 7A). Moreover, northern blot analysis showed the accumulation of a positive-sense RNA fragment of a size compatible with that of a subgenomic RNA originated by self-cleavage of the ribozyme (Supplementary Fig. 7B). Overall, experiments with total RNA purified from either infected plants or fungi followed by RACE analyses confirm that the population of viral RNAs *in vivo* is heterogeneous, being composed of uncleaved and self-cleaved RNA molecules.

Hammerhead ribozymes show a role in cap-independent translation initiation

Translation initiation activity, presumably via an internal ribosome entry site (IRES) element, has been reported *in vivo* for the 5'-UTR and subsequent 72 nt of coding region of fungal dsRNA viruses such as chrysoviruses and hypoviruses[43]. Among these, the 5'-UTR of the alphachrysovirus Helminthosporium victoriae virus 145S (HvV145S) RNA2 was found to carry an IRES element. We found that, as most alphachrysoviruses,

HvV145S RNA segments also contain a conserved type I hhrbz motif at their 5'-UTRs (Supplementary Table 1, Fig. 5A). These ribozymes correspond to the hhrbz variants with a long helix II (Fig. 2B), which are expected to reach significant self-cleaving activity *in vitro* and *in vivo*. To understand whether these type I hhrbzs are required to promote internal initiation of protein translation, on- and off-target mutations were introduced into the self-cleaving motif and analyzed *in vivo*. The transgenic expression of bicistronic RNAs in *C. parasitica* mycelia was carried out as previously described[43], in which the upstream ORluc and downstream OFluc were translated in cap- and IRES-dependent manner, respectively (Fig. 5B). The original HvV145S-2 5'-UTR sequence and its truncated variants in the 5' proximal region preceding the ribozyme (Δ60 and Δ120) showed similar ratios of OFluc to ORluc chemiluminescence intensity (RLU), suggesting that this off-target 5' region is dispensable for the IRES-mediated translation initiation (Fig. 5D). In contrast, the deletion of the whole region corresponding to the hhrbz motif (Δ124-183) abolished the IRES-mediated translation initiation of OFluc, resulting in a significantly lower OFluc/ORluc RLU ratio. In addition, either a point mutation in G159, the general base catalyst in the cleavage reaction[29], or deletion of 5 essential nucleotides, including the conserved U-turn motif[44] of the conserved core of the ribozyme (Δ134-138), abolished the translation initiation ability observed for the wt 5'-UTR sequence with a hhrbz (Fig. 5C and D).

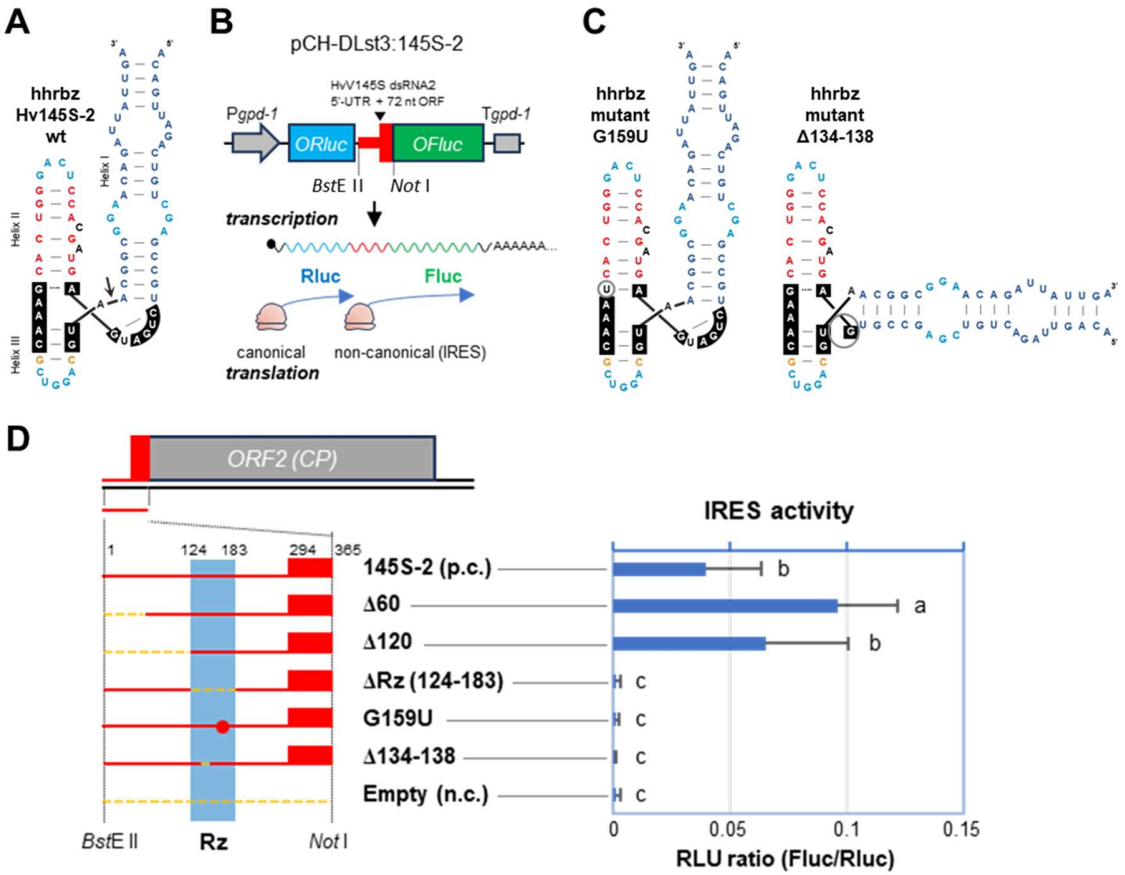

Fig. 5. Mutational analyses of the hammerhead ribozyme present in the 5'-UTR of the chrysovirus HvV145S RNA2. (A) Predicted structure of the HvV145S hammerhead ribozyme (hhrbz) present in the 5'-UTR of the RNA2. (B) A bicistronic dual-luciferase reporter system in fungal mycelia for investigation of the IRES function located at the 5'-UTR and coding region (72 nt) of HvV145S dsRNA2. Codon-optimized Renilla luciferase (ORluc, blue box) and firefly luciferase (OFluc, green box) genes are translated either in a canonical (cap-dependent) or a non-canonical (IRES-dependent) manner, respectively. Red line and box indicate HvV145S-2 sequence. (C) Predicted secondary structures of the 145S-2 hhrbz mutants containing either a substitution (left, G159U) or a deletion (right, Δ134-138), as indicated with grey circles. (D) Left, schematic representation of the 5'UTR and first 72 nt of coding region (in red) of HvV145S-2 (in grey) used for the bicistronic dual-luciferase reporter system. The details of mutations are represented at the bottom as the sequence variant names. Right, dual luciferase

reporter assay results for each construct showing the ratio of luminescent intensities (Fluc RLU/Rluc RLU=IRES activity). p.c., positive control, n.c., negative control.

Discussion

Almost four decades after their discovery, the origin and evolutionary history of small self-cleaving ribozymes remains a complex puzzle. It is assumed that RNAs capable of sequence-specific cleavage and ligation could be among the first catalytic motifs to emerge during the RNA world, with a role in processing primordial RNA and/or circRNA genomes during replication[45]. Our knowledge about small ribozymes has been mostly restricted to those from a tiny family of viroid-like circRNAs (~10-20 species), regarded as reminiscences of prebiotic genomes. In the last years, however, small catalytic RNAs have been found as ubiquitous motifs encoded in DNA genomes of organisms throughout the tree of life[16,46] and, more recently, as part of thousands of novel viroid-like circRNAs with unknown eukaryotic and, likely, prokaryotic hosts[30–33]. Thus, this plethora of catalytic motifs are expected to have more biological roles beyond multimer self-processing.

In this work, we have expanded our knowledge about the occurrence of small ribozymes to the linear genomes of typical ss- and dsRNA viruses of fungal origin. Notably, novel variants of the type I hhrbz are found to be conserved in many 5'-UTRs of fungal and plant RNA viruses of the *Chrysoviridae* and *Fusariviridae* families. It should be highlighted that nearly all hhrbz previously detected in infectious circRNAs, such as plant viroids and viral satellites[47], obelisks[48], deltaviruses[49], ambiviruses or mitoviruses[32,33], correspond to the type III architecture, whereas type I hhrbzs were so far DNA-encoded motifs found in either bacteriophages and bacteria[16,17,50] or eukaryotes (mostly in metazoan retroelements)[22,25,34]. On the other hand, natural hhrbzs adopt a similar three-way junction fold with loop-loop interactions between helixes I and II (Fig. 1), which are crucial to achieve high activity under *in vivo* low magnesium concentrations [28,29,51]. The viral type I hhrbzs described in this work, however, do not seem to have kept any of the typical loop-loop interactions conserved in known hhrbzs (Fig. 1) or in other three-helical RNAs with remote tertiary contacts[52].

Moreover, stem lengths of helix II in viral hhrbzs are either slightly longer (6-8 bp) or shorter (0-2 bp) (Fig. 2B) than the ones present in most type I hhrbzs (4-5 bp). These observations, together with a medium to low *in vitro* self-cleaving activity for viral hhrbzs, point to a lack of extensive loop-loop interactions in these motifs. These viral hhrbzs are however functional *in vivo*, as revealed by the co-existence of uncleaved and cleaved RNA genomes in plant and fungal infected cells, indicating that viral sub genomic RNAs can arise through a novel mechanism catalyzed by small self-cleaving ribozymes.

Regarding their biological role, most of the hhrbzs reported here are small motifs (50-70 nt), which nevertheless span a significant portion of the viral UTR sequences (~100-300 nt) where they are embedded. It is known that, among other functions, viral 5'-UTRs such as the one from HvV145S RNA2 (293 nt) can work as IRES elements[43]. Deletion mutants of this UTR show that the hhrbz motif (nucleotides 124-182) is required for IRES function. More intriguingly, a single mutation in the catalytic G base within the hhrbz core, which is known to inhibit RNA catalysis without dramatically affecting the whole ribozyme structure[53], was enough to drastically reduce the levels of protein expression obtained with the wt ribozyme-containing UTR. This result suggests that not only the ribozyme structure, but also its self-cleaving activity, would be crucial for the role of the UTR as an IRES. Consequently, we hypothesize that viral type I hhrbzs act as an IRES due to a combination of both ribozyme structure and self-cleaving activity, which may allow protein translation through an unknown mechanism. As a second alternative, we can also envisage that any mutation preventing self-cleavage is indeed affecting the global fold of the hhrbz, which could disrupt its role as an IRES. This possibility suggests that RNA self-cleavage could not be required for IRES function but, more likely, as negative regulator of translation. In either case, the central core of the hhrbz shows a clear secondary and tertiary structural similarity with the core domain of diverse IRES elements from picornaviruses[54] (Fig. 6). Regarding the 5'-UTR of the encephalomyocarditis virus (EMCV), it contains a type II IRES known to engage the translation initiation factor eIF4G through a three-helical motif known as the J-K region[55]. The structure of this motif shows a Y-shaped fold

without loop-loop interactions[56] but with a central core comparable to the one predicted for the hhrbz[29] (Fig. 6). The 5'-UTR of the Hepatitis A virus (HAV) has also a type III IRES composed of domains II to VI[57], with domain V (dV) as a core region structurally very similar[58] to the J-K region from EMCV or the hhrbz, and also capable of recruiting translation initiation factors such as eIF4G and eIF4F[59] (Fig. 6). As a last connection between protein translation and RNA self-cleaving motifs, it should be noted that the dvrbz present in the 5'-UTR of diverse eukaryotic retrotransposons has been found to promote protein translation initiation *in vitro* and *in vivo*[21]. Despite the structural differences between hhrbz and dvrbz (Supplementary Fig. 8), we cannot rule out a common and more general mechanism in protein translation for these and other self-cleaving RNAs.

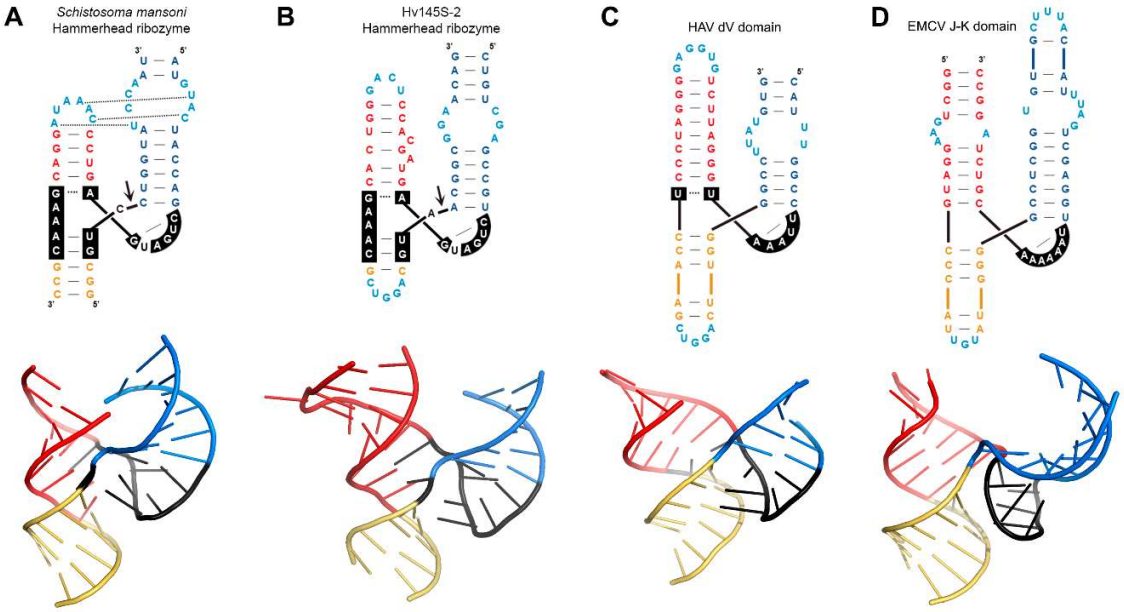

Fig. 6. (A) On the top, schematic representation of a type I hammerhead ribozyme (hhrbz) from *Schistosoma mansoni*. Tertiary loop-loop interactions are shown with dotted lines. On the bottom, 3D-structure (pdb 3ZD5) of the central core and the three stems, but not the loops, of this hhrbz (conserved core in black and stem I, II and III in blue, red and yellow, respectively). As above, similar schematic (top) and 3D structures (bottom) of (B) the Hv145S-RNA2 hhrbz (predicted through the Alphafold 3 server[60]), (C) Hepatitis A virus (HAV) IRES domain V (pdb 6mwn)[58] and (D) the J-K domain of the encephalomyocarditis virus (EMCV) IRES element (pdb 2nbx)[56].

Our discovery unveils an unexpected link between two unrelated kinds of ribozymes, such as simple self-cleaving RNAs and the complex ribosome. It could be argued that

this link may represent a primordial "interaction" dating back to the development of the genetic code, where the common presence of small self-cleaving ribozymes would be a selection force for their recognition by proto-ribosomes. Nevertheless, our observations are restricted for the moment to "modern" eukaryotic viruses, which are expected to have emerged after the origin of the eukaryotic cell itself (~2-3 billion years ago[61]). Moreover, the structural similarities of viral hhrbzs with some picornaviral IRES point to a recent event of domestication of the hhrbz to hijack translation initiation factors in eukaryotes instead of direct recruitment of the ribosome, as described for Hepatitis C virus (HCV) or cricket paralysis virus (CrPV) IRES elements[62,63]. While these groundbreaking findings offer valuable insights into RNA viral biology and potential biotechnological applications, further research will be needed to elucidate this intriguing viral mechanism of cap-independent translation mediated by small self-cleaving ribozymes.

Methods

Bioinformatic analysis of viral sequences

Computational searches through INFERNAL 1.1 software[64] were carried out using covariance models of well-known small ribozymes[33,65]. A first screening of a collection of 852 thousand contigs (between 2,000 and 50,000 bp) of DNA or RNA viral origin retrieved from the Genbank NR database resulted in hundreds of ribozyme hits that were manually inspected. Hits present in either viral vectors, patented sequences, DNA bacteriophages[16] or in RNA ambiviruses and mitoviruses[33] were discarded, whereas those hits with low E-values such as type I hammerhead (E-val < 10^{-3}), deltavirus (E-val < 0.1) or twister (E-val < 10^{-3}) ribozymes detected in RNA viruses from diverse families were used to build new covariance models and re-screenings (https://github.com/delapenya/RNA_virus_rbz). Analysis of specific RNA viral families showing the presence of small ribozymes and refinement of covariance models was performed iteratively.

The consensus features of the ribozyme motifs were calculated based on the obtained ribozyme sequences for each family. Nucleotide frequencies and covariation, as well as the corresponding drawing, were the output of the R2R software[66]. Multiple sequence alignments were performed using MUSCLE[67].

Cloning of ribozyme sequences and transcriptions

Sequences corresponding to the hhrbz motifs of the RNA 1 segments of Verticillium dahliae chrysovirus 1, Penicilium chrysogenum virus and Brassica campestris chrysovirus 1 (Fig. 3) preceded by the T7 RNA polymerase promoter were purchased as gBlock Gene Fragments (Integrated DNA Technologies). DNA fragments were cloned into a linearized pUC18 vector by BamHI and EcoRI cohesive-end ligation. RNAs of the cloned sequences were synthesized by *in vitro* run-off transcription of the linearized plasmids containing the hhrbzs. The transcription reactions contained 40 mM Tris–HCl, pH 8, 6 mM $MgCl_2$, 2 mM spermidine, 0.5 mg/ml RNase-free bovine serum albumin, 0.1% Triton X-100, 10 mM dithiothreitol, 1 mM each of ATP, CTP, GTP, and UTP, 2 U/µl of Ribonuclease Inhibitor (Takara Inc), 20 ng/µl of plasmid DNA, and 4 U/µl of T7 RNA polymerase. After incubation at 37°C during the indicated time, the products were fractionated by 10% polyacrylamide gel electrophoresis (PAGE) in the presence of 8 M urea.

Kinetics of self-cleavage

Analyses of hhrbz self-cleavage activity under co-transcriptional and post-transcriptional conditions were performed as previously described[68]. Appropriate aliquots of the transcription reactions (smaller volumes were taken at longer incubation times in co-transcriptional assays) were removed at different time intervals, quenched with a fivefold excess of stop solution (8 M urea, 50% formamide, 50 mM EDTA, 0.1% xylene cyanol and bromophenol blue) at 0°C, and analyzed as previously described[22,49]. For co-transcriptional cleavage analysis, the uncleaved and

cleaved transcripts obtained at different times were separated by PAGE in 10% denaturing gels and detected by Sybr Gold staining (Thermo Fisher Scientific). For post-transcriptional cleavage analysis, uncleaved primary transcripts were eluted by crushing the gel pieces and extracting them with phenol saturated with buffer (Tris–HCl 10 mM, pH 7.5, ethylenediaminetetraacetic acid [EDTA] 1 mM, sodium dodecyl sulfate 0.1%), recovered by ethanol precipitation, and resuspended in deionized sterile water. To determine the cleaving rate constants, uncleaved primary transcripts (from 1 nM to 1 µM) were incubated in 20 µl of 50 mM Tris–HCl at the appropriate pH (either 7,5 or 8,5) for 1 min at 95 °C and slowly cooled to 25 °C for 15 min. After taking a zero-time aliquot, self-cleavage reactions were triggered by adding $MgCl_2$ at a final concentration of either 1 or 10 mM. Aliquots were removed at the appropriate time intervals and quenched with a fivefold excess of stop solution at 0 °C. Substrate and self-cleaved products were separated by PAGE in 10% denaturing gels and detected by Sybr Gold staining (Thermo Fisher Scientific). In both cases, the product fraction at different times, Ft, was determined by quantitative scanning of the corresponding gel bands and fitted to the equation $F_t=F_\infty(1 - e^{-kt})$, where F_∞ is the product fraction at the reaction endpoint, t is the time in minutes, and k is the first-order rate constant of cleavage (k_{obs}).

RACE and northern blot analyses

Analysis of fusarivirus-infected fungi was carried out using the isolate MUT4379 from the Mycotheca Universitatis Taurinensis. Gnomognopsis castanea chrysovirus 1 infected isolate 1 was recently described[41]. A symptomless plant of cabbage “Torzella” (*Brassica oleracea* L. var. acephala) infected with BcCV1 (isolate TC-3) was used for plant chysovirus 5’ RACE analysis[69].

Plant and fungal total RNA was extracted from leaves from cabbage “Torzella” plants and 4-day old mycelial liquid cultures grown in PDB following protocols previously described[41,69]. Hirtzman’s protocol for RACE was performed as previously described in detail[70]. For each RACE two primers were designed downstream the predicted

ribozyme cleavage site. Regarding GcCV1, the primers used to demonstrate the *in vivo* activity of the ribozymes found in the 5' end of each genomic segment are reported in a previous work[41]. For the RACE demonstrating the *in vivo* activity of the ribozyme found in the intergenic region of the RNA3 of GcCV1, two RACE primers were designed (Supplementary Table 2); the oligonucleotides used to prime RACE for PtFV1 and BcCV1 are also displayed in Supplementary Table 2. For each RACE a minimum of 5 clones were sequenced.

Northern blot of fungal extracts for MUT4379 was performed as previously described[71] using a riboprobe (detecting the positive sense viral RNA) obtained by *in vitro* transcription of a cDNA fragment cloned into pGEM-T-Easy (PROMEGA, Madison, WI) corresponding to the genomic region between nt 4,800 and nt 4,980 of the deposited fusarivirus sequence (NCBI NC_028470).

Dual-luciferase (DL) reporter assay

The DL assay using fungal mycelia was performed as previously described[43]. Briefly, the pCH-DLst3 vector and PCR-amplified fragments of 5'-UTR and adjacent 72 nt of coding sequence (5'-UTR+) from HvV145S dsRNA2 were digested with BstE II and Not I, and ligated. The clone obtained was used for transformation of *Chryphonectria parasitica* EP155, and mycelia of transformants were subjected to the DL assay as described[43].

The vector pCH-DLst3 carries a codon-optimized Renilla luciferase (ORluc) and a Firefly luciferase (OFluc) gene in a bicistronic manner, under the control of the gpd-1 promoter/terminator system. BstE II and Not I recognition sites in between ORluc and OFluc were used for inserting the 5'-UTR and adjacent 72 nt coding cDNA sequence (5'-UTR+; original and mutant variants), expecting that ORluc and OFluc are translated cap- and IRES-dependently, respectively. *C. parasitica* EP155 was transformed with the different constructs and mycelia of transformants were subjected to DL assay using a dual-luciferase reporter assay system (Promega). A small patch of mycelia was homogenized in a microtube with 200 µl of Cell-Lysate solution, and 10 µl of solution

were mixed with 100 µl of the firefly luciferase substrate solution, then the first luminescence intensity was measured using GloMax 20/20 (Promega) with a detection time of 1 s. This was followed by the addition of 100 µl of the Renilla luciferase substrate solution, and the second luminescence measurement. IRES activities were calculated as a ratio of Fluc RLU (relative luminescent unit)/ Rluc RL.

Supplementary Figures and Tables

Supplementary Table 1. Accession numbers of all the RNA virus genomes/segments containing self-cleaving ribozymes identified in this study.

EXCEL FILE

Supplementary Table 2. Oligonucleotide sequences and their specific use in this work.

Oligonucleotide Name	Sequence (5' to 3')	Use
BcCV1-RNA1-77Rev	CAAAGATGCGTTTTCCCATGC	RACE
BcCV1-RNA1-87Rev	TGCTTTGCAGCACCGTTTA	RACE
BcCV1-RNA1-88NRev	TCGTCTGTGTAGCAACACTAAC	RACE
BcCV1-RNA2-81Rev	GCGCAAGCAACCAGGTTCA	RACE
BcCV1-RNA2-82Rev	CCTTCCATTGTGCTATTAAGGTAT	RACE
BcCV1-RNA3-85Rev	CTCTTCATGTTGCATGAATTCG	RACE
BcCV1-RNA3-86Rev	TGCAGACGTGTTTTCCATTGT	RACE
Fusari-5000Rev	TGTTTCCTTGACGCTCGTGT	RACE
Fusari-4800For	ACCCGGAGAGCTCAAATGTT	RACE
Fusari-4980Rev	GTAACTTAAGAAGTTTGGCT	RACE
GcCV1_RNA3_1163Rev	AATCTCTCCGCCGCTGTCGT	RACE
GcCV1_RNA3_1104Rev	TGTTCTCCCGTTCCTCGGTG	RACE

Supplementary Figures

Supplementary Fig. 1. (A) Detailed consensus models and secondary structures of the hammerhead ribozymes either with long helix II (left, based on 26 ribozyme sequences) or short helix II (right, based on 62 ribozyme sequences) from chrysovirus genomes. (B) Consensus model of the hammerhead ribozyme present in most fusarivirus genomes (based on 123 ribozyme sequences). The legend inset applies to the three models shown. (C) Three representative examples of hammerhead ribozymes from fusarivirus genomes with variable stem lengths for helix I, II and III. The site of ribozyme-mediated RNA cleavage is identified by an arrowhead. Consensus models were built as previously described[66].

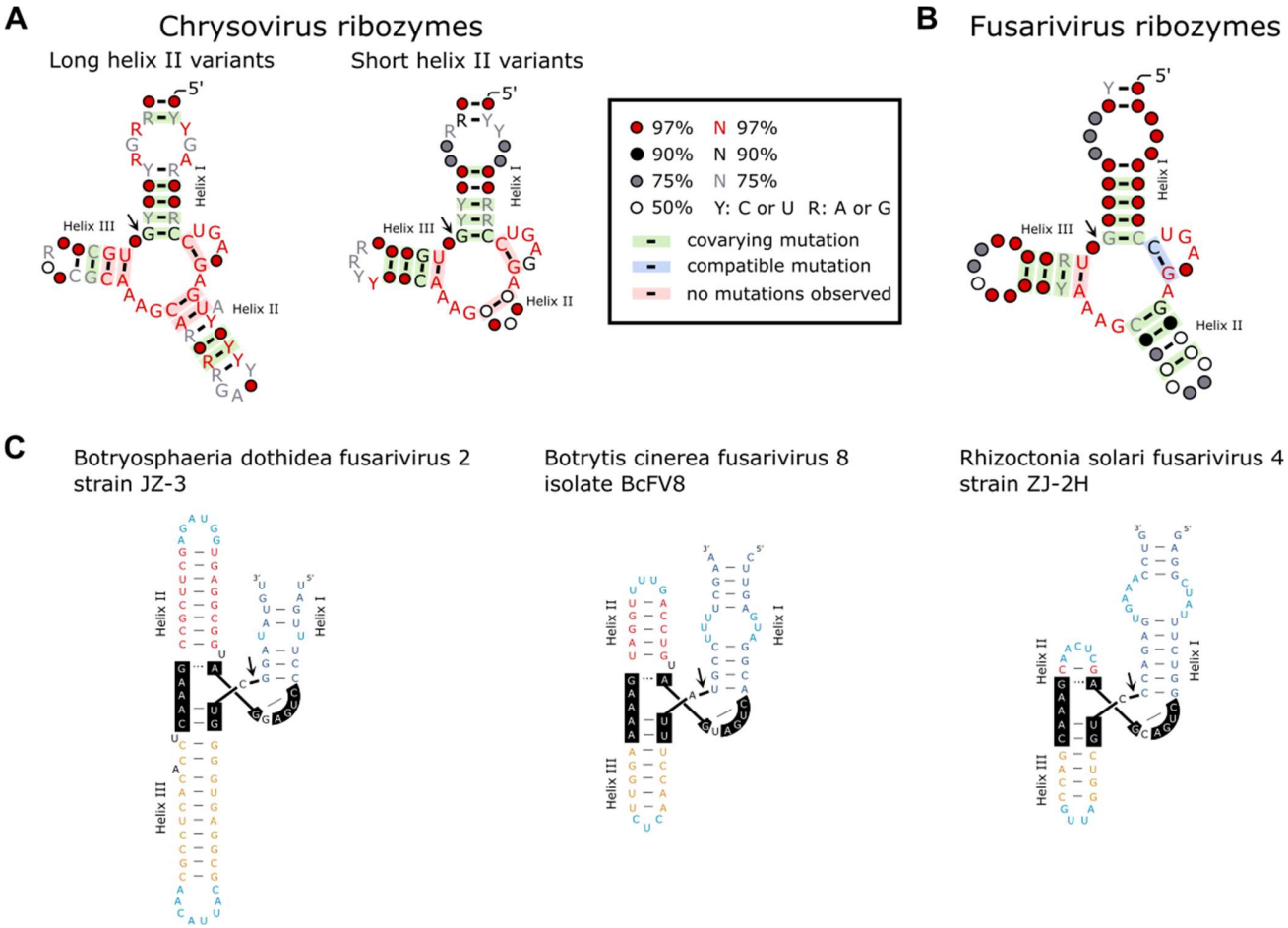

Supplementary Fig. 2. Representative assays of self-cleavage kinetics for three hammerhead ribozymes encoded in fungal and plant chrysoviruses. (A) Structure of the hammerhead ribozyme from Verticillium dahliae chrysovirus 1, RNA 1 (left), a 10% PAGE showing the resulting RNAs after different transcription times (standard conditions, pH 7.5, 1 mM Mg^{2+}) (center), and the kinetic analysis and quantification graph of the cleavage rates under these co-transcriptional conditions (right). (B) Structure of the hammerhead ribozyme from Penicillium chrysogenum virus, RNA 1 (left), a 10% PAGE showing a post-transcriptional assay of self-cleavage with purified RNA of this ribozyme incubated at pH 8.5 and 1 or 10 mM Mg^{2+}(Methods) (right), and their kinetic analysis and quantification graph of the observed cleavage rates (bottom). (C) Structure of the hammerhead ribozyme from Brassica campestris chrysovirus (left), two 10% PAGEs showing post-transcriptional assays of self-cleavage with purified RNA of this ribozyme incubated at pH 8.5 and 1 or 10 mM Mg^{2+}(Methods) (right), and their kinetic analysis and quantification graph of the cleavage rates (bottom).

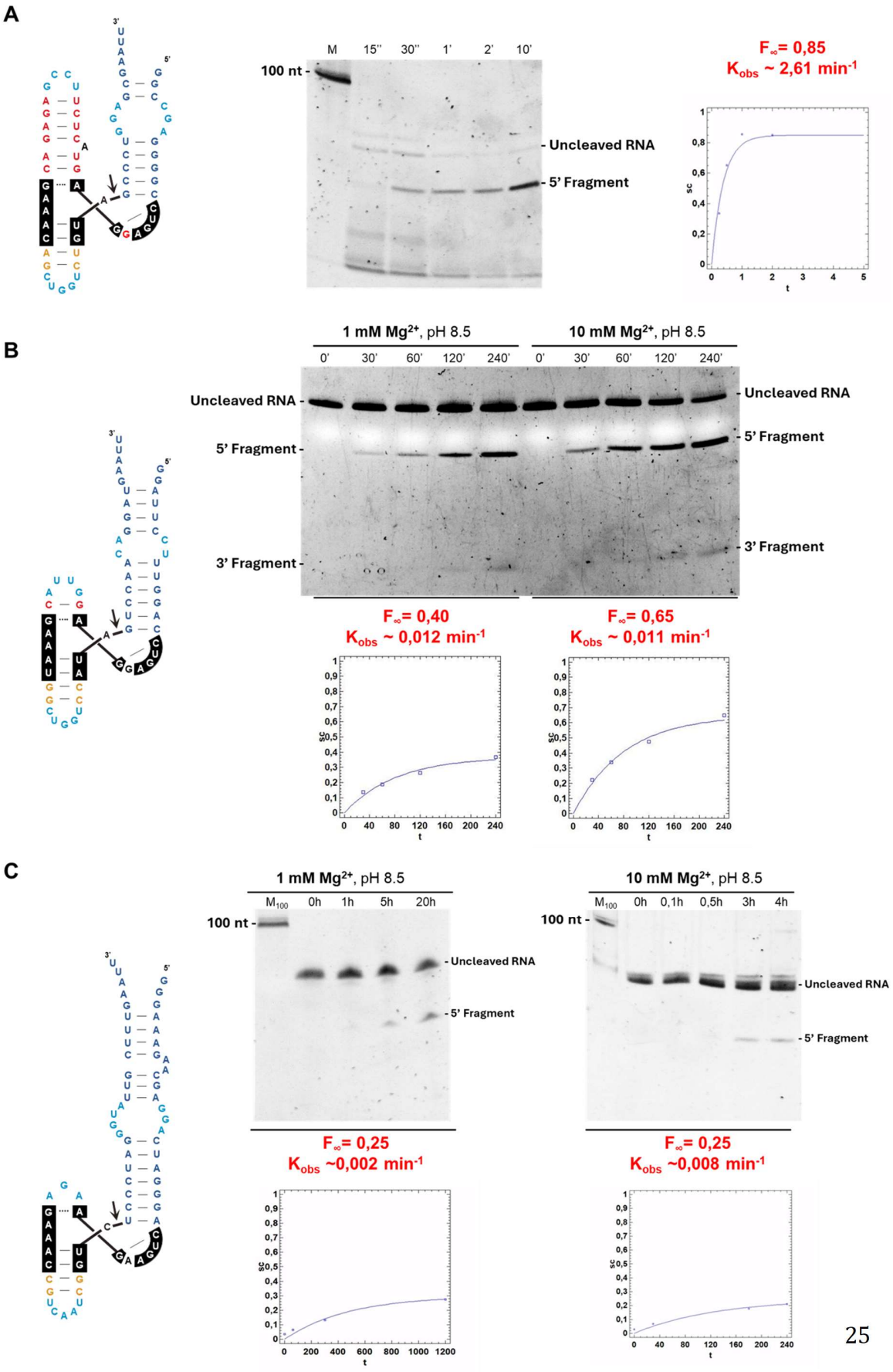

512

Supplementary Fig. 3. (A) Representative examples of hammerhead ribozymes (hhrbzs) detected in the UTRs of two ssRNA fusariviruses. (B) An example of a dsRNA megabirnavirus-like genome showing the presence of a hhrbz in its 5'-UTR and a deltavirus ribozyme encoded within the predicted RNA dependent RNA polymerase (RdRp) ORF. Sites of ribozyme self-cleavage are indicated by arrows.

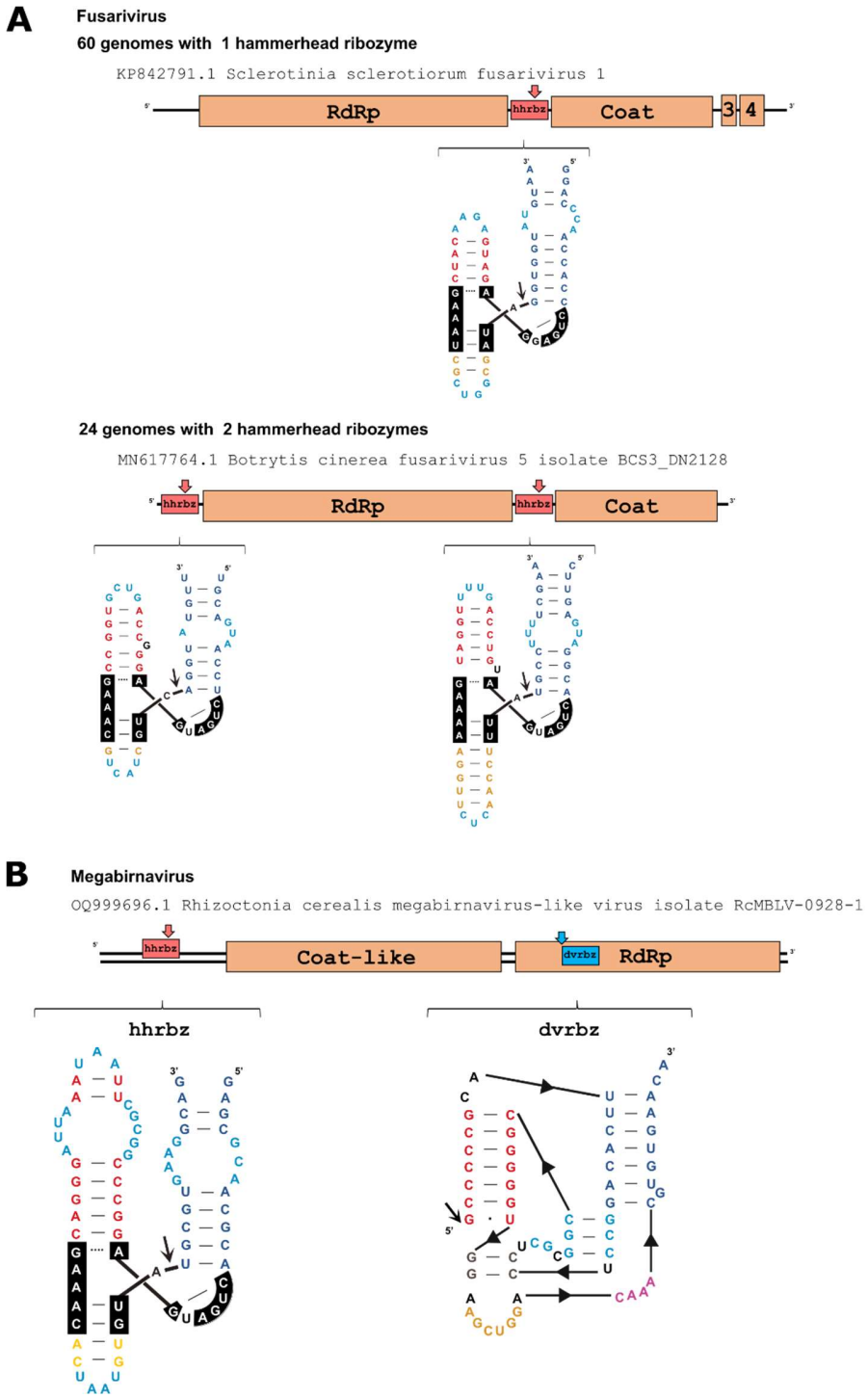

Supplementary Fig. 4. Subgenomic circular RNAs (circRNAs) produced by closely located tandem ribozyme pairs are likely encoded in some totivirids and similar RNA virus genomes. The small RNA fragments resulting after ribozyme self-cleavage usually show a nucleotide size multiple of 3, potentially encode an endless ORF (absence of stop codons) in the viral polarity, and are predicted to be highly base-paired circRNAs similar to viroid-like agents, zeta-viruses[30] or those encoded by eukaryotic retrozymes[24,25]. Hyp; hypothetical. polyprot; polyprotein. hhrbz; hammerhead ribozyme. dvrbz; deltavirus ribozyme. RdRp; RNA dependent RNA polymerase.

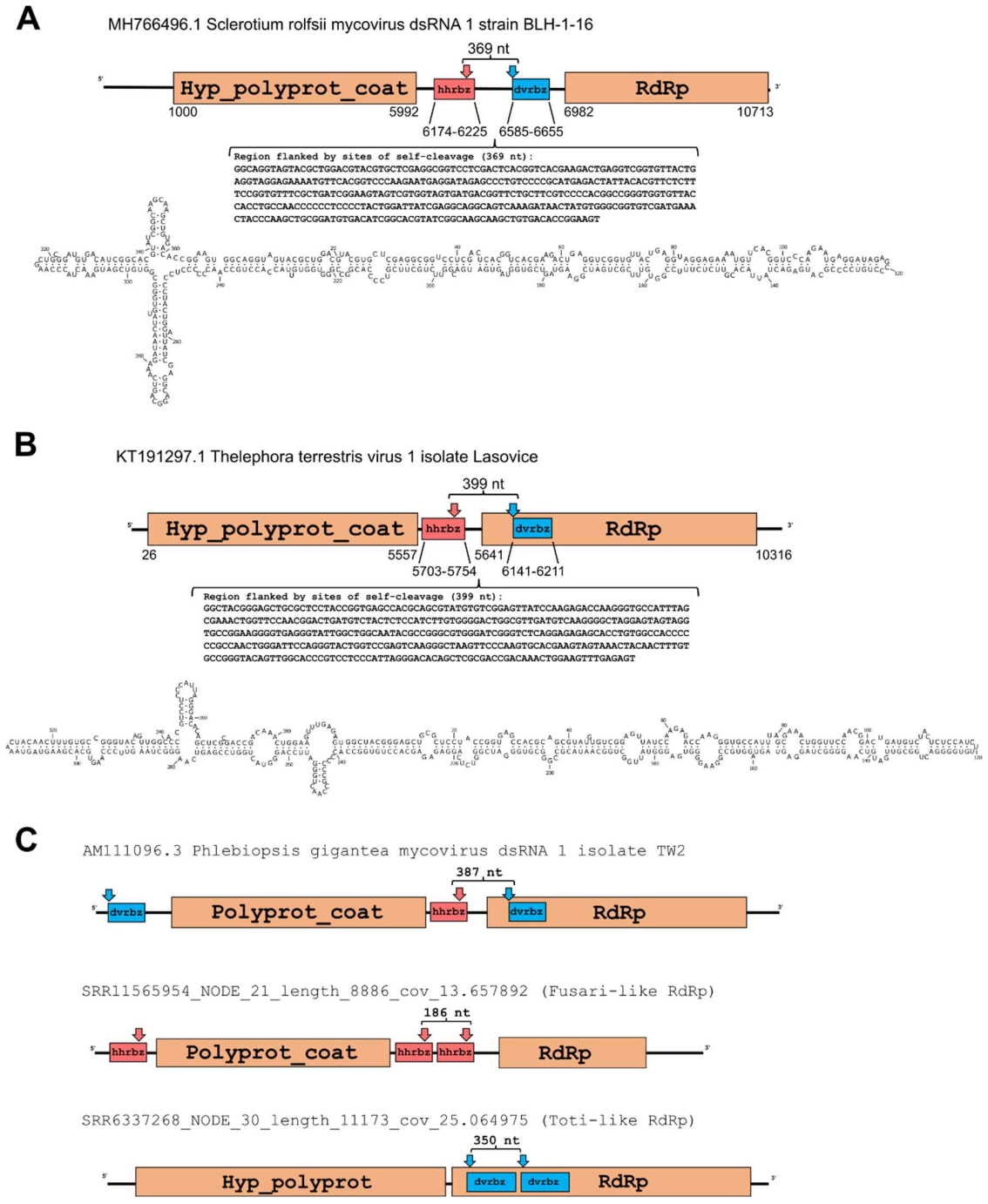

Supplementary Fig. 5. 5' RACE of Brassica campestris chrysovirus 1 (BcCV-1) from infected cabbage Torzella plants. (A) Schematic representation of the BcCV-1 hhrbzs in the 5'-UTRs of each of the three genomic RNA segments. (B) Agarose gel analysis of 5' RACE PCR of BcCV-1 RNA1, RNA2 and RNA3 (lanes 1, 2 and 3, respectively) shows two bands corresponding to the amplification of the full-length (upper and more abundant band) and the self-cleaved (lower band) RNAs. For the RNA1 (lane 1), a nested PCR, using a reverse BcCV-1 RNA1 (BcCV1-RNA1-88NRev, Supplementary Table S2), nested to the primer used in the first RACE amplification (BcCV1-RNA1-87Rev, Supplementary Table S2), is shown. M, DNA molecular weight marker (100 bp DNA ladder, Thermo Fisher). (C) Sequencing electropherograms of the cloned RACE product of smaller size for each RNA genomic segment. The 5' end coincides with that predicted to be generated by the hhrbz self-cleavage (indicated by arrows).

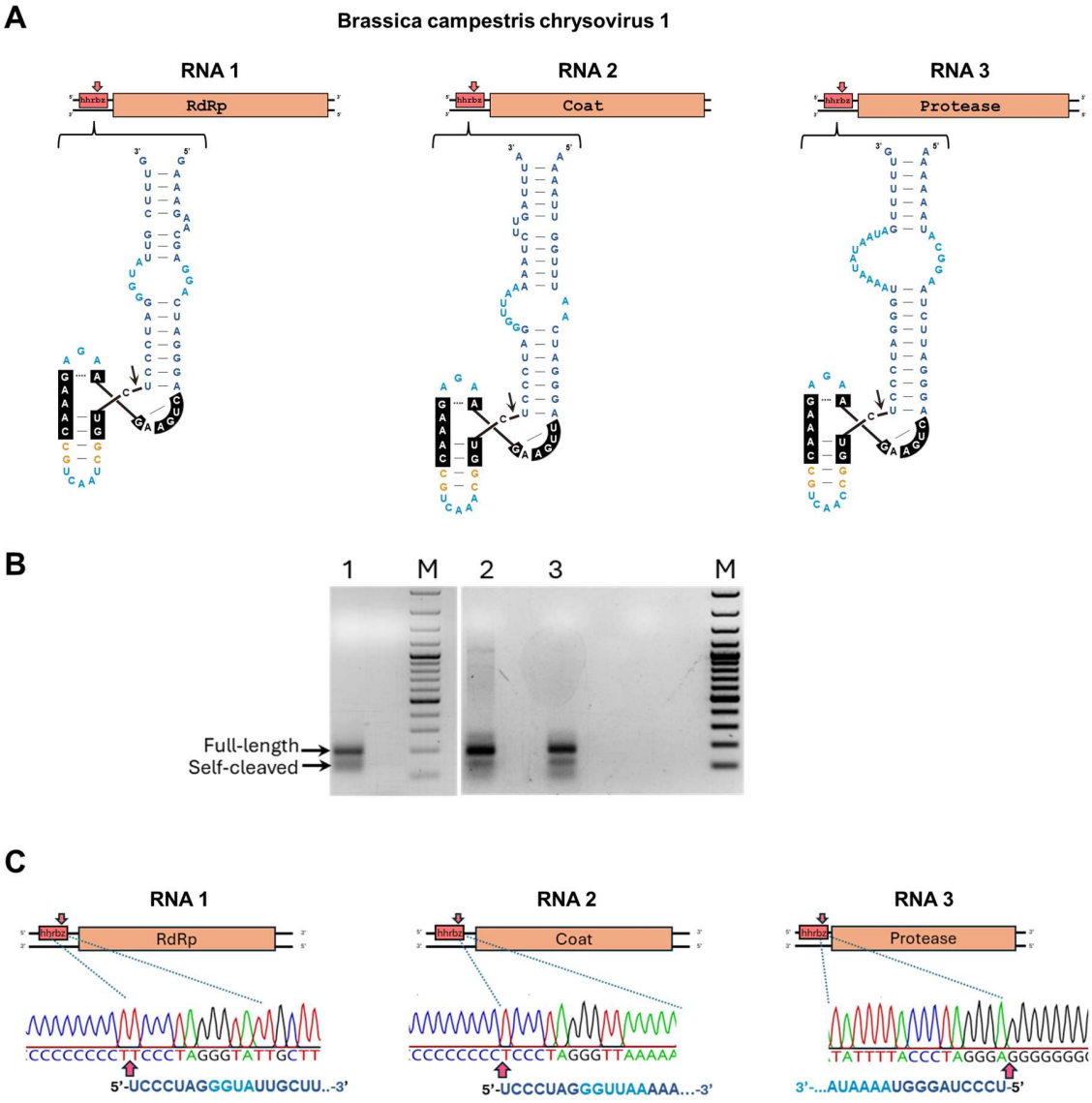

Supplementary Fig. 6. 5' RACE of Gnomoniopsis castaneae chrysovirus 1 (GcCV-1) from infected *G. castaneae* isolate 1[41]. Schematic representation of GcCV-1 RNAs, hammerhead ribozymes (hhrbz) secondary structure and sequencing electropherograms of the cloned RACE product of smaller size for each (A) RNA 1, (B) RNA 2 (C) RNA 3 and (D) RNA 4 genomic segments. Hhrbzs are present in all the 5'-UTR of RNAs, whereas RNA3 shows a second intergenic hhrbz motif between the two conserved ORFs (3a and 3b). The 5' ends of the sequencing electropherograms coincide with those predicted to be generated by the hhrbz self-cleavage (indicated by arrows). (E) Agarose gel analysis of 5' RACE PCR (lane 1) and 3'RACE PCR (lane 2) of GcCV-1 RNA2. Lane 1 shows two bands corresponding to the amplification of the full-length (upper band) and the self-cleaved (lower band) RNAs. M; DNA molecular weight marker of 100 bp DNA (Thermo Fisher). RdRp; RNA dependent RNA polymerase. CP; coat protein. ORF; open reading frame.

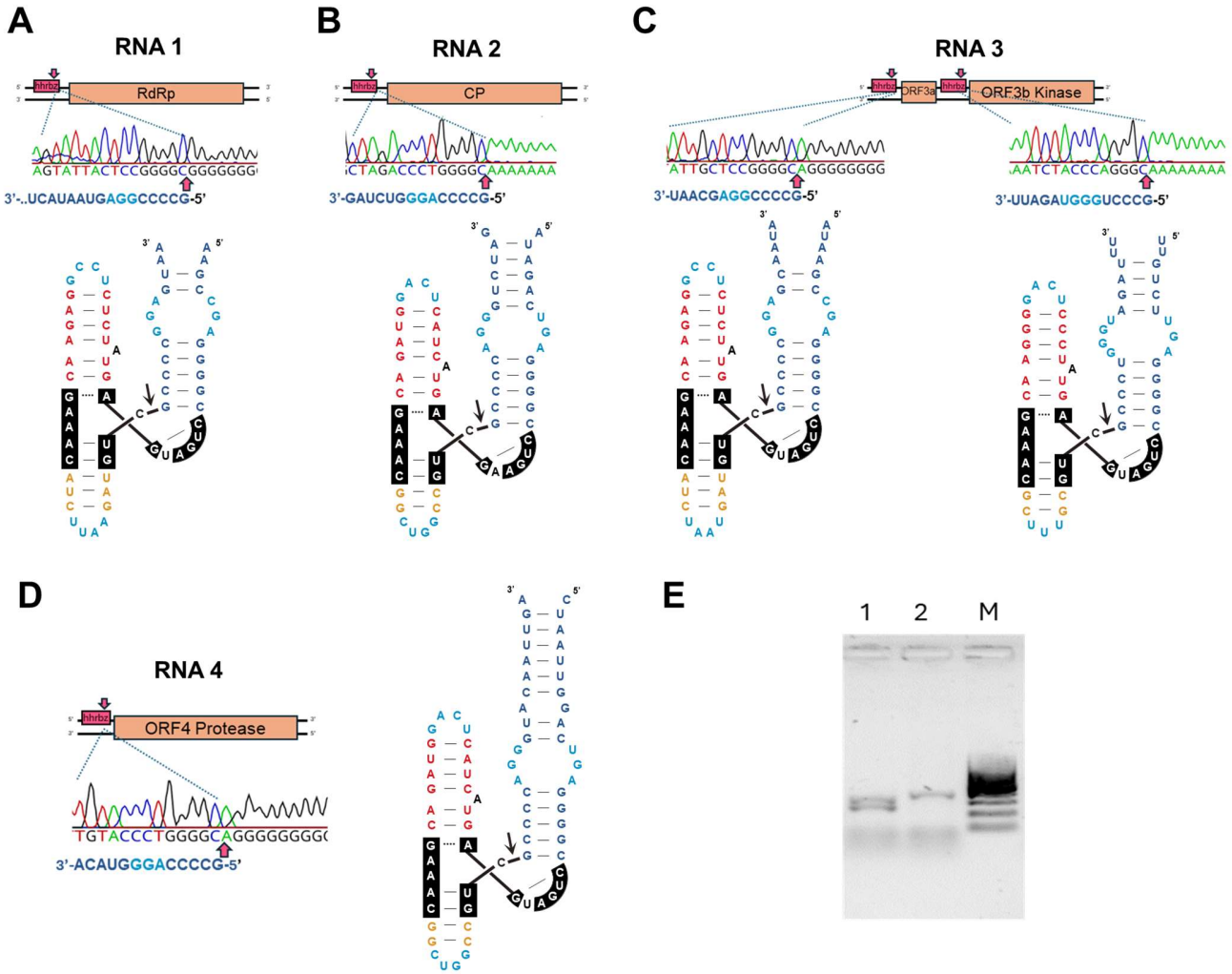

Supplementary Fig. 7. 5' RACE of Pleospora typhicola fusarivirus 1 (PtFV1) from infected MUT 4379 [42]. (A) Genome organization, with the position of the hammerhead ribozyme (hhrbz) placed in the intergenic region. The secondary structure of the ribozyme is also displayed (right), as well as the sequence electropherogram showing the 5' end of the cleavage site (red arrow). (B) Northern blot analysis of RNA extracts from virus-infected isolate MUT4379 and virus-free *Rhizoctonia solani* isolate IEE-16[72]. On the left panel, red arrows indicate the PtFV1 genomic RNA (gRNA) and PtFV1 sgRNA positions, while green arrows indicate some possible cross-hybridization with the two fungal ribosomal RNAs. The right panel shows a methylene blue stain of the membrane displaying the two ribosomal RNA bands.

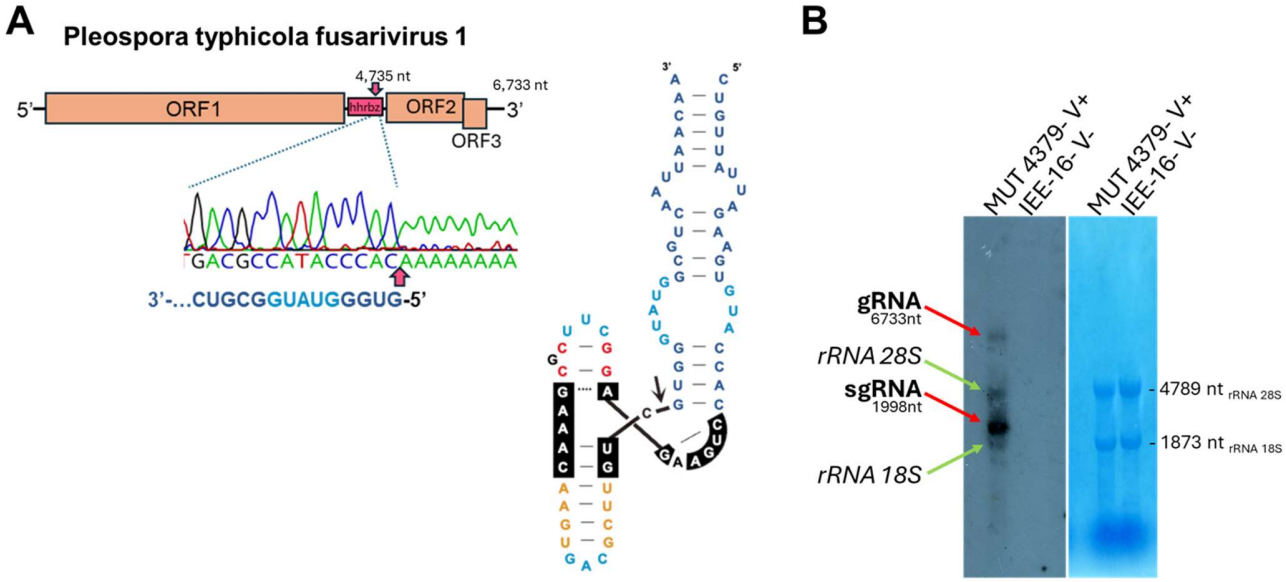

569 **Supplementary Fig. 8**. Three dimensional models for (A) the hammerhead ribozyme
570 from *Schistosoma mansoni* retrozymes (pdb 3ZD5, only central core and stems, loops 1
571 and 2 not shown), (B) the human Hepatitis Delta ribozyme (pdb 1DRZ), (C) the
572 Hepatitis A virus IRES dV domain (pdb 6mwn) and (D) the encephalomyocarditis virus
573 IRES J-K domain (pdb 2nbx).

574

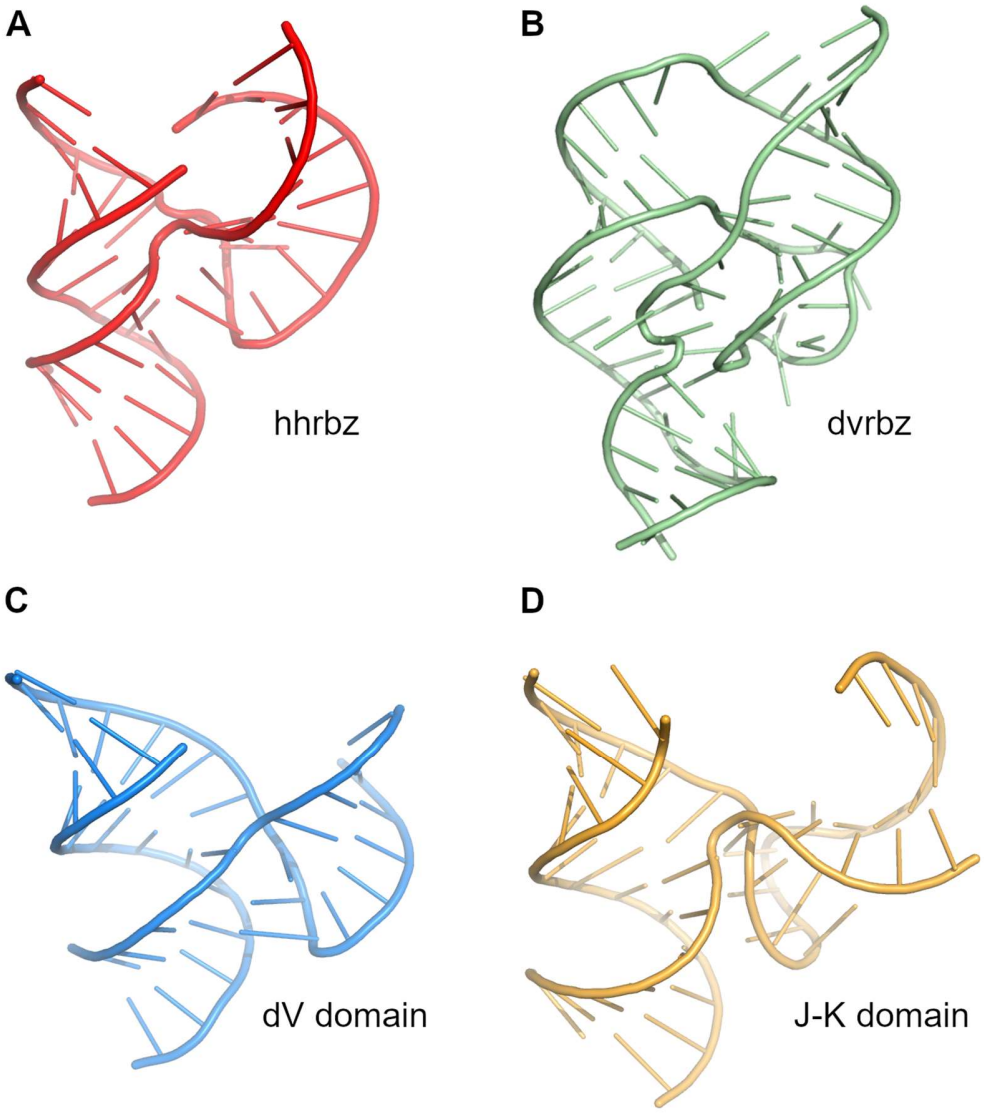

575

576

Acknowledgments

This work was funded by: University of Valencia Margarita Salas Fellowship MS21-067 (MJLG); Generalitat Valenciana Grant PROMETEO CIPROM/2022/21 (MdlP); Ministry of Economics and Competitivity of Spain-FEDER grant PID2020-116008GB-I00 (MdlP). We are grateful to Daniela Alio and Maria Minutolo for providing plants infected by Brassica campestris chrysovirus 1.

References

1. Woese, C. R. The fundamental nature of the genetic code: prebiotic interactions between polynucleotides and polyamino acids or their derivatives. *Proc Natl Acad Sci U S A* **59**, 110–117 (1968).

2. Crick, F. H. The origin of the genetic code. *J Mol Biol* **38**, 367–379 (1968).

3. Gilbert, W. The RNA World. *Nature* **319**, 618 (1986).

4. Flores, R., Gago-Zachert, S., Serra, P., Sanjuan, R. & Elena, S. F. Viroids: survivors from the RNA world? *Annu Rev Microbiol* **68**, 395–414 (2014).

5. Forterre, P. The origin of viruses and their possible roles in major evolutionary transitions. *Virus Res* **117**, 5–16 (2006).

6. Prody, G. A., Bakos, J. T., Buzayan, J. M., Schneider, I. R. & Bruening, G. Autolytic processing of dimeric plant virus satellite RNA. *Science (1979)* **231**, 1577–1580 (1986).

7. Hutchins, C. J., Rathjen, P. D., Forster, A. C. & Symons, R. H. Self-cleavage of plus and minus RNA transcripts of avocado sunblotch viroid. *Nucleic Acids Res* **14**, 3627–3640 (1986).

8. Buzayan, J. M., Gerlach, W. L. & Bruening, G. Satellite tobacco ringspot virus RNA: A subset of the RNA sequence is sufficient for autolytic processing. *Proc Natl Acad Sci U S A* **83**, 8859–8862 (1986).

9. Kuo, M. Y., Sharmeen, L., Dinter-Gottlieb, G. & Taylor, J. Characterization of self-cleaving RNA sequences on the genome and antigenome of human hepatitis delta virus. *J Virol* **62**, 4439–4444 (1988).

10. Saville, B. J. & Collins, R. A. A site-specific self-cleavage reaction performed by a novel RNA in Neurospora mitochondria. *Cell* **61**, 685–696 (1990).

11. Winkler, W. C., Nahvi, A., Roth, A., Collins, J. A. & Breaker, R. R. Control of gene expression by a natural metabolite-responsive ribozyme. *Nature* **428**, 281–286 (2004).

12. Roth, A. *et al.* A widespread self-cleaving ribozyme class is revealed by bioinformatics. *Nat Chem Biol* **10**, 56–60 (2014).

13. Weinberg, Z. *et al.* New classes of self-cleaving ribozymes revealed by comparative genomics analysis. *Nat Chem Biol* **11**, 606–610 (2015).

14. Ferbeyre, G., Smith, J. M. & Cedergren, R. Schistosome satellite DNA encodes active hammerhead ribozymes. *Mol Cell Biol* **18**, 3880–3888 (1998).

15. Epstein, L. M. & Gall, J. G. Self-cleaving transcripts of satellite DNA from the newt. *Cell* **48**, 535–543 (1987).

16. Hammann, C., Luptak, A., Perreault, J. & de la Peña, M. The ubiquitous hammerhead ribozyme. *RNA* **18**, 871–885 (2012).

17. De la Peña, M. & García-Robles, I. Ubiquitous presence of the hammerhead ribozyme motif along the tree of life. *RNA* **16**, 1943–1950 (2010).

18. Webb, C. H. T., Riccitelli, N. J., Ruminski, D. J. & Lupták, A. Widespread occurrence of self-cleaving ribozymes. *Science (1979)* **326**, 953 (2009).

19. De la Peña, M. & Garcia-Robles, I. Intronic hammerhead ribozymes are ultraconserved in the human genome. *EMBO Rep* **11**, 711–716 (2010).

20. Salehi-Ashtiani, K., Luptak, A., Litovchick, A. & Szostak, J. W. A genomewide search for ribozymes reveals an HDV-like sequence in the human CPEB3 gene. *Science (1979)* **313**, 1788–1792 (2006).

21. Ruminski, D. J., Webb, C. H. T., Riccitelli, N. J., Lupta, A. & Luptak, A. Processing and translation initiation of non-long terminal repeat retrotransposons by hepatitis delta virus (HDV)-like self-cleaving ribozymes. *J Biol Chem* **286**, 41286–41295 (2011).

22. Cervera, A. & de la Peña, M. Eukaryotic penelope-like retroelements encode hammerhead ribozyme motifs. *Mol Biol Evol* **31**, 2941–2947 (2014).

23. Eickbush, D. G. & Eickbush, T. H. R2 retrotransposons encode a self-cleaving ribozyme for processing from an rRNA cotranscript. *Mol Cell Biol* **30**, 3142–3150 (2010).

24. Cervera, A., Urbina, D. & de la Peña, M. Retrozymes are a unique family of non-autonomous retrotransposons with hammerhead ribozymes that propagate in plants through circular RNAs. *Genome Biol* **17**, 135 (2016).

25. Cervera, A. & de la Peña, M. Small circRNAs with self-cleaving ribozymes are highly expressed in diverse metazoan transcriptomes. *Nucleic Acids Res* **48**, 5054–5064 (2020).

26. Liu, G. *et al.* The function of twister ribozyme variants in non-LTR retrotransposition in Schistosoma mansoni. *Nucleic Acids Res* **49**, 10573–10588 (2021).

27. Salehi-Ashtiani, K. & Szostak, J. W. In vitro evolution suggests multiple origins for the hammerhead ribozyme. *Nature* **414**, 82–84 (2001).

28. De la Peña, M., Gago, S. & Flores, R. Peripheral regions of natural hammerhead ribozymes greatly increase their self-cleavage activity. *EMBO J* **22**, 5561–5570 (2003).

29. Martick, M. & Scott, W. G. Tertiary contacts distant from the active site prime a ribozyme for catalysis. *Cell* **126**, 309–320 (2006).

30. Edgar, R. C. *et al.* Petabase-scale sequence alignment catalyses viral discovery. *Nature 2022* **602**, 1–6 (2022).

31. Weinberg, C. E., Olzog, V. J., Eckert, I. & Weinberg, Z. Identification of over 200-fold more hairpin ribozymes than previously known in diverse circular RNAs. *Nucleic Acids Res* **49**, 6375–6388 (2021).

32. Lee, B. D. *et al.* Mining metatranscriptomes reveals a vast world of viroid-like circular RNAs. *Cell* **186**, 646-661.e4 (2023).

33. Forgia, M. *et al.* Hybrids of RNA viruses and viroid-like elements replicate in fungi. *Nature Communications 2023 14:1* **14**, 1–11 (2023).

34. Arkhipova, I. R., Yushenova, I. A. & Rodriguez, F. Giant Reverse Transcriptase-Encoding Transposable Elements at Telomeres. *Mol Biol Evol* **34**, 2245–2257 (2017).

35. Epstein, L. M. & Pabon-Pena, L. M. Alternative modes of self-cleavage by newt satellite 2 transcripts. *Nucleic Acids Res* **19**, 1699–1705 (1991).

36. Cao, Y. fen *et al.* Genomic characterization of a novel dsRNA virus detected in the phytopathogenic fungus Verticillium dahliae Kleb. *Virus Res* **159**, 73–78 (2011).

37. Zhang, R. *et al.* A novel single-stranded RNA virus isolated from a phytopathogenic filamentous fungus, Rosellinia necatrix, with similarity to hypo-like viruses. *Front Microbiol* **5**, 92402 (2014).

38. Chiba, S. *et al.* ICTV Virus Taxonomy Profile: Fusariviridae 2024: This article is part of the ICTV Virus Taxonomy Profiles collection. *Journal of General Virology* **105**, 001973 (2024).

677 39. Chiba, S. *et al.* A novel bipartite double-stranded RNA mycovirus from the white
678 root rot fungus Rosellinia necatrix: Molecular and biological characterization,
679 taxonomic considerations, and potential for biological control. *J Virol* **83**,
680 12801–12812 (2009).

681 40. Zhang, J. *et al.* The genome sequence of Brassica campestris chrysovirus 1, a
682 novel putative plant-infecting tripartite chrysovirus. *Arch Virol* **162**, 1107–
683 1111 (2017).

684 41. Ferilli, F., Lione, G., Gonthier, P., Turina, M. & Forgia, M. First detection of
685 mycoviruses in Gnomoniopsis castaneae suggests a putative horizontal gene
686 transfer event between negative-sense and double-strand RNA viruses.
687 *Virology* 110057 (2024) doi:10.1016/J.VIROL.2024.110057.

688 42. Nerva, L. *et al.* Multiple approaches for the detection and characterization of
689 viral and plasmid symbionts from a collection of marine fungi. *Virus Res* **219**,
690 22–38 (2016).

691 43. Chiba, S., Jamal, A. & Suzuki, N. First evidence for internal ribosomal entry sites
692 in diverse fungal virus genomes. *mBio* **9**, (2018).

693 44. Doudna, J. A. Hammerhead ribozyme structure: U-turn for RNA structural
694 biology. *Structure* **3**, 747–750 (1995).

695 45. Kristoffersen, E. L., Burman, M., Noy, A. & Holliger, P. Rolling Circle RNA
696 Synthesis Catalysed by RNA. *Elife* **11**, (2022).

697 46. Jimenez, R. M., Polanco, J. A. & Luptak, A. Chemistry and Biology of Self-Cleaving
698 Ribozymes. *Trends Biochem Sci* **40**, 648–661 (2015).

699 47. De la Peña, M., Garcia-Robles, I. & Cervera, A. The Hammerhead Ribozyme: A
700 Long History for a Short RNA. *Molecules* **22**, 1–11 (2017).

701 48. Zheludev, I. N. *et al.* Viroid-like colonists of human microbiomes. *bioRxiv*
702 2024.01.20.576352 (2024) doi:10.1101/2024.01.20.576352.

703 49. De La Peña, M., Ceprian, R., Casey, J. L. & Cervera, A. Hepatitis delta virus-like
704 circular RNAs from diverse metazoans encode conserved hammerhead
705 ribozymes. *Virus Evol* **7**, (2021).

706 50. Perreault, J. *et al.* Identification of hammerhead ribozymes in all domains of life
707 reveals novel structural variations. *PLoS Comput Biol* **7**, e1002031 (2011).

708 51. Khvorova, A., Lescoute, A., Westhof, E. & Jayasena, S. D. Sequence elements
709 outside the hammerhead ribozyme catalytic core enable intracellular activity.
710 *Nat Struct Biol* **10**, 708–712 (2003).

52. De la Peña, M., Dufour, D. & Gallego, J. Three-way RNA junctions with remote tertiary contacts: a recurrent and highly versatile fold. *RNA* **15**, 1949–1964 (2009).

53. Schultz, E. P., Vasquez, E. E. & Scott, W. G. Structural and catalytic effects of an invariant purine substitution in the hammerhead ribozyme: Implications for the mechanism of acid-base catalysis. *Acta Crystallogr D Biol Crystallogr* **70**, 2256–2263 (2014).

54. Martínez-Salas, E., Francisco-Velilla, R., Fernandez-Chamorro, J., Lozano, G. & Diaz-Toledano, R. Picornavirus IRES elements: RNA structure and host protein interactions. *Virus Res* **206**, 62–73 (2015).

55. Kolupaeva, V. G., Pestova, T. V., Hellen, C. U. T. & Shatsky, I. N. Translation Eukaryotic Initiation Factor 4G Recognizes a Specific Structural Element within the Internal Ribosome Entry Site of Encephalomyocarditis Virus RNA. *Journal of Biological Chemistry* **273**, 18599–18604 (1998).

56. Imai, S., Kumar, P., Hellen, C. U. T., D'Souza, V. M. & Wagner, G. An accurately preorganized IRES RNA structure enables eIF4G capture for initiation of viral translation. *Nature Structural & Molecular Biology 2016 23:9* **23**, 859–864 (2016).

57. Brown, E. A., Day, S. P., Jansen, R. W. & Lemon, S. M. The 5' nontranslated region of hepatitis A virus RNA: secondary structure and elements required for translation in vitro. *J Virol* **65**, 5828–5838 (1991).

58. Koirala, D. *et al.* A conserved RNA structural motif for organizing topology within picornaviral internal ribosome entry sites. *Nature Communications 2019 10:1* **10**, 1–13 (2019).

59. Avanzino, B. C., Fuchs, G. & Fraser, C. S. Cellular cap-binding protein, eIF4E, promotes picornavirus genome restructuring and translation. *Proc Natl Acad Sci U S A* **114**, 9611–9616 (2017).

60. Abramson, J. *et al.* Accurate structure prediction of biomolecular interactions with AlphaFold 3. *Nature 2024* 1–3 (2024) doi:10.1038/s41586-024-07487-w.

61. Strassert, J. F. H., Irisarri, I., Williams, T. A. & Burki, F. A molecular timescale for eukaryote evolution with implications for the origin of red algal-derived plastids. *Nature Communications 2021 12:1* **12**, 1–13 (2021).

62. Fernández, I. S., Bai, X. C., Murshudov, G., Scheres, S. H. W. & Ramakrishnan, V. Initiation of Translation by Cricket Paralysis Virus IRES Requires Its Translocation in the Ribosome. *Cell* **157**, 823–831 (2014).

63. Pfingsten, J. S., Costantino, D. A. & Kieft, J. S. Structural basic for ribosome recruitment and manipulation by a viral IRES RNA. *Science (1979)* **314**, 1450–1454 (2006).

64. Nawrocki, E. P. & Eddy, S. R. Infernal 1.1: 100-fold faster RNA homology searches. *Bioinformatics* **29**, 2933–2935 (2013).

65. Kalvari, I. *et al.* Rfam 14: expanded coverage of metagenomic, viral and microRNA families. *Nucleic Acids Res* **49**, D192–D200 (2021).

66. Weinberg, Z. & Breaker, R. R. R2R - software to speed the depiction of aesthetic consensus RNA secondary structures. *BMC Bioinformatics* **12**, 1–9 (2011).

67. Edgar, R. C. MUSCLE: multiple sequence alignment with high accuracy and high throughput. *Nucleic Acids Res* **32**, 1792–1797 (2004).

68. Long, D. M. & Uhlenbeck, O. C. Kinetic characterization of intramolecular and intermolecular hammerhead RNAs with stem II deletions. *Proc Natl Acad Sci U S A* **91**, 6977–6981 (1994).

69. Minutolo, M. *et al.* A polyvalent tool for detecting coguviruses in multiple hosts allowed the identification of a novel seed-transmitted coguvirus infecting Brassicaceae. *Phytopathology* (2023) doi:10.1094/PHYTO-10-23-0362-R/ASSET/IMAGES/LARGE/PHYTO-10-23-0362-RT2.JPEG.

70. Rastgou, M. *et al.* Molecular characterization of the plant virus genus Ourmiavirus and evidence of inter-kingdom reassortment of viral genome segments as its possible route of origin. *J Gen Virol* **90**, 2525 (2009).

71. Sutela, S. *et al.* The virome from a collection of endomycorrhizal fungi reveals new viral taxa with unprecedented genome organization. *Virus Evol* **6**, (2020).

72. Picarelli, M. A. S. C. *et al.* Extreme diversity of mycoviruses present in isolates of rhizoctonia solani AG2-2 LP from Zoysia japonica from Brazil. *Front Cell Infect Microbiol* **9**, 457597 (2019).